A Thermo-elastic Annular Plate Model for the Modeling of Brake Systems*

José Luis Reyes Pérez◇, Andreas Heckmann◇ and Ingo Kaiser◇
◇German Aerospace Center (DLR), Institute of Robotics and Mechatronics
Oberpfaffenhofen, 82234 Wessling, Germany

Abstract

The friction forces generated during braking between brake pads and discs produce high thermal gradients on the rubbing surfaces. These thermal gradients may cause braking problems such as brake fade, premature wear or hot spotting and the associated hot judder phenomenon in the frequency range below 100 Hz.

Further consequences are comfort reductions, a defective braking process, inhomogeneous wear, cutbacks of the brake performance and even damage of brake components.

The present paper proposes a modeling concept that is targeted on this field of application and introduces the new Modelica class ThermoelasticPlate, which is implemented in the DLR FlexibleBodies library.

Keywords: Disc brake, Modal multifield approach, Thermoelasticity

1 Introduction

Friction braking is necessarily related to high thermal loads which lead to high temperatures at the surface of brake discs and to large thermal gradients as well. The friction forces in turn depend on temperature, on load and sliding speed [1] so that the braking performance and the related wear phenomena are known to be ruled by a complex interrelationship.

In addition, the thermal loads can initiate the onset of unevenly distributed hot spots or bands and thermally deformed brake discs [2], [3]. Since the brake pads then slide upon a non-smooth surface while the brake disc rotates, the brake system vibrates, noise is generated and undesirable wear occurs.

Due to the conduction of heat to other components such as the caliper, the bearing or the brake fluid further performance reducing or even dangerous effects such as brake fluid boiling and vaporization have been reported by several authors, see e.g. [4].

Besides experimental studies the finite element method (FEM) [5], [6], [7] [8] or analytical techniques [9] [10] are utilized to analyze the thermal and thermo-elastic behavior of brakes in literature.

Both methods have advantages and provide valuable results, but both methods are not well suited, if complex scenarios such as the interaction of brakes with suspensions or vehicle control systems are investigated and a system dynamical point of view is adopted.

To this purpose the present paper proposes a novel model of a moderately simplified brake disc. Depending on the user input the thermo-elastic behavior of brake discs is described with approximately 100 up to 1000 degrees of freedom.

The thermal field of the disc is discretized in three dimensions and the associated states are specified likewise in Lagrangian or in Eulerian representation. An annular Kirchhoff plate is adapted to evaluate the deformations according to the uncoupled thermo-elastic theory [11, Ch. 2] presuming that the mechanical terms in the heat conduction equations are negligible.

In circumferential direction the disc is assumed to be rotational symmetric, in axial direction different layers with different heat capacity and conduction properties and multiple surfaces, where cooling by convection occurs, may be defined.

In order to implement this concept the Modelica class ThermoelasticPlate has been introduced into the commercial DLR FlexibleBodies library. This paper presents the underlying theory on thermal and thermo-elastic fields, explains the user interface of the ThermoelasticPlate class and gives a simulation example. The final section gives an outlook to further efforts in research and modeling of friction brakes and its validation, which is supposed to be initiated by the novel

*Updated and revised version of the paper published at the 8th International Modelica Conference, March 20-22, 2011, Dresden.

modeling approach.

2 Thermal Field

2.1 Weak Field Equations

In order to describe the thermal behaviour of the brake disc the weak equations for the temperature field $\vartheta(\boldsymbol{c},t)$ as functions of the spatial position in cylindrical coordinates $\boldsymbol{c} = (r,\phi,z)^T$ and time t are deduced from the principle of virtual temperature, see e.g. [12, (7.7)] or [13, (1.3.33)]:

$$\int_V [-(\nabla\delta\vartheta)^T \boldsymbol{q} + \rho c\,\dot{\vartheta}\delta\vartheta]\,\mathrm{d}V + \ldots \\ \ldots + \int_B \boldsymbol{q}_B^T \boldsymbol{n}_B \delta\vartheta\,\mathrm{d}B = 0\,, \tag{1}$$

where ρ denotes the density, c the specific heat capacity, $\mathrm{d}B$ the boundary element and $\boldsymbol{n}_B$ the outer unit normal vector. $\boldsymbol{q}$ symbolizes the heat flux according to Fourier's law of heat conduction depending on the temperature gradient $\nabla\vartheta$ and the thermal conductivity matrix $\boldsymbol{\Lambda}$ [11, (1.12.16)]:

$$\boldsymbol{q} = -\boldsymbol{\Lambda}\nabla\vartheta \tag{2}$$

The boundary heat flux q_B may be given explicitly or, if convection occurs, may be specified by the film coefficient h_f and the bulk temperature ϑ_∞ of the fluid [11, Sec. 5.6]:

$$\boldsymbol{q}_B^T \boldsymbol{n}_B = -q_B - h_f(\vartheta_B - \vartheta_\infty)\,. \tag{3}$$

2.2 Modal Approach

The discretization of the scalar temperature is performed using the Ritz approximation that allows to separate the thermal field description by a finite-dimensional linear combination of two parts, the first one considers thermal modes and is spatial dependent, i.e. $\boldsymbol{\Phi}_\vartheta = \boldsymbol{\Phi}_\vartheta(\boldsymbol{c})$ and the second one represent the modal amplitudes and is time dependent, i.e. $\boldsymbol{z}_\vartheta = \boldsymbol{z}_\vartheta(t)$:

$$\vartheta(\boldsymbol{c},t) = \boldsymbol{\Phi}_\vartheta(\boldsymbol{c})\boldsymbol{z}_\vartheta(t) \tag{4}$$

The spatial mode functions are formulated using the separation approach of Bernoulli for the spatial coordinates as well, so that (4) may be rewritten as follows:

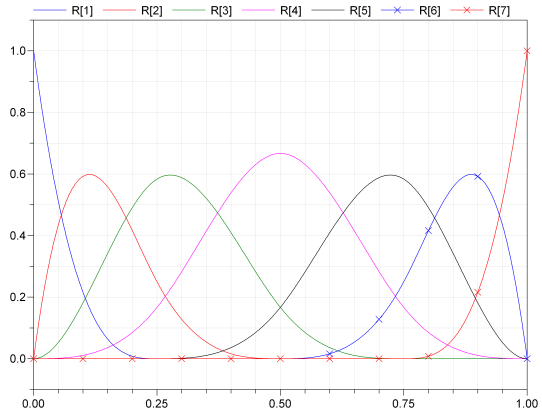

Figure 1: Example set of B-splines to discretize the thermal field in radial and axial direction.

$$\sum_{i=1}^{n} \Phi_{\vartheta i}(\boldsymbol{c}) z_{\vartheta i}(t) = \sum_{i=1}^{n} R_i(r)\,\Psi_i(\phi)\,Z_i(z)\,z_{\vartheta i}(t) = \\ = \sum_{l=1}^{l_m}\sum_{k=0}^{k_m}\sum_{m=1}^{m_m} R_l(r)\cdot\cos(k\phi)\cdot Z_m(z)\cdot z_{\vartheta i}(t) + \\ + \sum_{l=1}^{l_m}\sum_{k=1}^{k_m}\sum_{m=1}^{m_m} R_l(r)\cdot\sin(k\phi)\cdot Z_m(z)\cdot z_{\vartheta i}(t)\,, \\ \text{with } i = 1,2,\ldots,n\,,\ n = (l_m m_m)(2k_m+1)\,. \tag{5}$$

According to *Walter Ritz* [14], the trial functions have to be linearly independent and components of a complete system, so that the number of i may be increased as needed in order to improve the approximation. For $R_l(r)$ and $Z_m(z)$ B-splines [15] as shown in Fig. 1 have been chosen as trial functions in radial and axial direction, respectively.

The harmonic waves (or Fourier series expansion) $\Psi_i(\phi)$ are appropriate in circumferential direction, since

- they allow to represent cyclic properties, i.e. $\Psi_i(\phi) = \Psi_i(\phi + 2\pi)$,
- they are simple to integrate from 0 to 2π,
- their orthogonality leads to block-diagonal system matrices, i.e. the entire system of equations is split up into decoupled sub-systems,
- they will later on be exploited to provide a Eulerian description of the thermo-elastic plate.

2.3 Discretized Field Equations

If (5) is inserted into (1), the volume integrals can be separated from the terms that dependent on time. As a

result, the linear thermal field equation is obtained:

$$\boldsymbol{C}_{\vartheta\vartheta}\dot{\boldsymbol{z}}_\vartheta + (\boldsymbol{K}_{\vartheta\vartheta} + \boldsymbol{K}_{\vartheta R})\boldsymbol{z}_\vartheta = \boldsymbol{Q}_{\vartheta N}\, q_B + \boldsymbol{Q}_{\vartheta R}\,\vartheta_\infty\,, \quad (6)$$

where the volume integrals are defined, inter alia using the abbreviation $\boldsymbol{B}_\vartheta := \nabla\boldsymbol{\Phi}_\vartheta$, as follows [16, Tab. 2.5]:

the heat capacity matrix:	$\boldsymbol{C}_{\vartheta\vartheta} := \int_V \rho c\, \boldsymbol{\Phi}_\vartheta^T \boldsymbol{\Phi}_\vartheta \,\mathrm{d}V$
the conductivity matrix:	$\boldsymbol{K}_{\vartheta\vartheta} := \int_V \boldsymbol{B}_\vartheta^T \boldsymbol{\Lambda} \boldsymbol{B}_\vartheta \,\mathrm{d}V$
the Robin load matrix:	$\boldsymbol{K}_{\vartheta R} := \int_B h_f\, \boldsymbol{\Phi}_\vartheta^T \boldsymbol{\Phi}_\vartheta \,\mathrm{d}B$
the Robin load vector:	$\boldsymbol{Q}_{\vartheta R} := \int_B h_f\, \boldsymbol{\Phi}_\vartheta^T \,\mathrm{d}B$
the Neumann load vector:	$\boldsymbol{Q}_{\vartheta N} := \int_B \boldsymbol{\Phi}_\vartheta^T \,\mathrm{d}B$

These volume integrals may therefore be evaluated in advance to the simulation or time integration, respectively.

Note, that neither (6) nor (1) comprehend terms that express the thermodynamics of deformations, so the so-called thermo-elastic damping phenomenon is disregarded [11, Ch. 2]. This approach is commonly known as uncoupled thermo-elastic theory, which nevertheless covers heat energy dissipation of mechanical processes. Indeed, e.g. friction initiates an associated heat flux q_B and therefore enters (6) as external load $\boldsymbol{Q}_{\vartheta N}\boldsymbol{q}_B$ which corresponds to Neumann boundary conditions in the partial differential equation related to (6).

2.4 The Eulerian Description

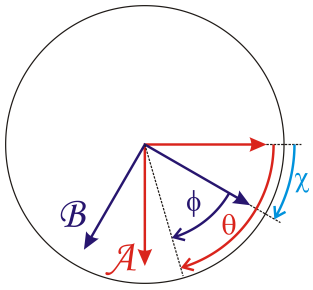

Figure 2: Coordinate transformation with angle χ, that leads from the Lagrangian to the Eulerian description.

It is now considered that the brake disc performs a rotation around its central axis specified by the angle $\chi(t)$. So far the temperature field is described in the so-called Lagrangian point of view [17, Sec. I.3], i.e. the reference frame follows the rotation as it is shown for the coordinate system named $\mathcal{B}$ in Fig. 2.

However for the specific use case treated here it may make sense to resolve the temperature field of the disc in frame $\mathcal{A}$ in Fig. 2. In other words, the observer does not rotate with the disc but looks on the plate from the outside, from a point in rest concerning the rotation with angle $\chi(t)$.

This concept is the so-called Eulerian description [17, Sec. I.4] and is widely used in fluid dynamics, where the motion state of the fluid at a fixed point in space is presented. Due to the rotational symmetry properties of the brake disc the Eulerian description can here be formulated in an elegant and convenient way.

For theoretical derivation the coordinate transformation

$$\phi = \theta - \chi \quad (7)$$

is defined, where θ specifies the angular position of an observed point on the brake disc resolved with respect to the Eulerian reference system $\mathcal{A}$ in Fig. 2.

Furthermore it is assumed that for every trial function in (5) that employs a $\sin(k\phi)$-term an associated trial function is present where the sinus- is replaced by the cosinus-function only, but $R_l(r)$, $Z_m(z)$ and k are identical, so that mode shape couples c_1 and c_2 exist:

$$\begin{aligned} c_1(r,\phi,z) &= R_l(r)\cdot Z_m(z)\cdot\sin(k\phi)\,, \\ c_2(r,\phi,z) &= R_l(r)\cdot Z_m(z)\cdot\cos(k\phi)\,. \end{aligned} \quad (8)$$

If the following identities

$$\begin{aligned} \sin(k\phi) &= \sin(k\theta)\cos(k\chi) - \cos(k\theta)\sin(k\chi)\,, \\ \cos(k\phi) &= \cos(k\theta)\cos(k\chi) + \sin(k\theta)\sin(k\chi) \end{aligned} \quad (9)$$

are inserted into (8), an associated mode couple $\bar{c}_1(r,\theta,z)$ and $\bar{c}_2(r,\theta,z)$ defined with respect to frame $\mathcal{A}$ appears:

$$\begin{aligned} c_1 = \underbrace{R_l Z_m \sin(k\theta)}_{:=\bar{c}_1(r,\theta,z)}\cos(k\chi) - \\ \underbrace{R_l Z_m \cos(k\theta)}_{:=\bar{c}_2(r,\theta,z)}\sin(k\chi)\,, \quad (10) \\ c_2 = \bar{c}_1(r,\theta,z)\sin(k\chi) + \bar{c}_2(r,\theta,z)\cos(k\chi)\,. \end{aligned}$$

As a result of suitable transformations it may also be written:

$$\begin{aligned} \bar{c}_1(r,\theta,z) &= c_2\sin(k\chi) + c_1\cos(k\chi)\,, \\ \bar{c}_2(r,\theta,z) &= c_2\cos(k\chi) - c_1\sin(k\chi)\,. \end{aligned} \quad (11)$$

The mode functions $\bar{c}_1(r,\theta,z)$ and $\bar{c}_2(r,\theta,z)$ are defined in the Eulerian reference system $\mathcal{A}$ and are linear combinations of the mode functions $c_1(r,\phi,z)$ and $c_2(r,\phi,z)$ described in the Lagrangian frame $\mathcal{B}$, whereas the combination depends on $\chi(t)$.

This information can be exploited in order to define a transformation: a thermal field resolved in the Lagrangian frame can be transformed to be resolved in the Eulerian frame and vice versa. Of course the physical temperature field itself does not change, but its resolution does so that the numerical values describing the field will be different in frame $\mathcal{A}$ or $\mathcal{B}$, respectively.

In practice the transformation is formulated in terms of the modal amplitudes $z_{\vartheta i}(t)$ which are the thermal states in (6):

$$\begin{aligned} \bar{z}_{\vartheta i1}(t) &= \sin(k\chi(t))z_{\vartheta i2}(t) + \cos(k\chi(t))z_{\vartheta i1}(t)\ , \\ \bar{z}_{\vartheta i2}(t) &= \cos(k\chi(t))z_{\vartheta i2}(t) - \sin(k\chi(t))z_{\vartheta i1}(t)\ . \end{aligned} \tag{12}$$

Again, the new modal amplitudes in the Eulerian frame $\bar{z}_{\vartheta i}(t)$ are expressed as a linear combination of modal amplitudes in the Lagrangian frame $z_{\vartheta i}(t)$ and it is just a matter of convenience and practicability in which coordinates the thermal field equations are actually evaluated.

One particularity has been ignored so far. For trial functions with $k = 0$ no mode couple with c_1 and c_2 according to (8) exists, since no associated sinus-function is introduced in (5). As a consequence the transformation (12) is not defined for such modes. However, trial functions with $k = 0$ represent rotational symmetric fields since the dependency on ϕ is eliminated in (5) due to the term $\cos(k\phi)$. As a consequence mode shapes with $k = 0$ are invariant with respect to rotations with angle χ or in other words: The modal coordinates $z_{\vartheta i}(t)$ related to $k = 0$ are identical in the Eulerian and the Lagrangian description and no transformation is needed.

3 Mechanical Field

The present paper is focused on the thermo-elastic interrelation that rules the behavior of brake discs in the low frequency range. Note that there is a complementary paper presented on this Modelica User Conference which is dedicated to higher frequencies in order to cope e.g. with brake squeal phenomena [18]. However here, it is supposed that the excitation is much lower than the lowest natural frequency of the brake disc. In particular the following assumption are made:

- The structural deformations of the brake disc are dominated by its elasticity or thermo-elasticity, respectively. Inertia effects are out of focus and in particular the influence of the brake disc rotation on the deformations are negligible. This statement is related to the so-called Duhamel's assumption which argues on the different timescales with which changes in the temperature or deformation field usually proceed, cp. [11, Sec. 2.5].
- A literature review on the characteristics of thermo-elastic brake disc deformation give reason to the assumption that plate bending in some cases even plate buckling is the governing deformation mechanism, see [9], [2], [6]. For example: all experimental studies describe e.g. hot spots to be located alternatively on the two disc surfaces in anti-symmetrical configuration, so that the circumference is deformed similar to a sinuous line. Therefore the deformation field of the brake disc here is represented as an annular Kirchhoff plate.

Note that the description of the annular plate is limited to be linear in this initial implementation, so that plate buckling phenomena are not covered, see [19], [20, Ch. 1]. An extended formulation to consider thermal buckling is a field of active research at the DLR.

3.1 Thermo-elastic Coupling

In [16, Sec. 2.2] the material constitution based on a thermodynamical potential is harnessed to formulate the interrelation of the thermal and the mechanical field. This approach is not suited here, since the influence of a 3-dimensional thermal on a 2-dimensional displacement field is to describe.

Instead the so-called body-force analogy is employed, i.e. the thermo-elastic problem is transfered into an isothermal problem with equivalent distributed body forces $\boldsymbol{\sigma}_\vartheta$ [11, §3.3], whose non-zeros components in radial and tangential direction read:

$$\boldsymbol{\sigma}_{\vartheta r} = \boldsymbol{\sigma}_{\vartheta\phi} = -\frac{1+\nu}{1-\nu^2} E\alpha\,\vartheta\ , \tag{13}$$

where α denotes the thermal expansion coefficient, E Young's modulus and ν the Poisson number. Together with the relevant strain components in radial and tangential direction ε_r and ε_ϕ expressed as functions of the transversal plate deformation w

$$\varepsilon_r = -z\,w_{,rr}\ , \qquad \varepsilon_\phi = -z\left(\frac{w_{,r}}{r} + \frac{w_{,\phi\phi}}{r^2}\right)\ , \tag{14}$$

the associated virtual work δW_ϑ reads:

$$\begin{aligned} \delta W_\vartheta &= \int_V \delta\varepsilon^T \boldsymbol{\sigma}_\vartheta\,\mathrm{d}V = \\ &= \int_V E\alpha\frac{1+\nu}{1-\nu^2}\,\delta\begin{pmatrix} w_{,rr} \\ \frac{w_{,r}}{r} + \frac{w_{,\phi\phi}}{r^2} \end{pmatrix}^T \begin{pmatrix} z\,\vartheta \\ z\,\vartheta \end{pmatrix} \mathrm{d}V \end{aligned} \tag{15}$$

3.2 Weak Field Equations

The structural displacements $\boldsymbol{u}$ are evaluated on the basis of the principle of virtual displacements [12, (4.7)], which states that the virtual work of the internal forces equals the virtual work of the interia and external forces:

$$\int_V \delta\varepsilon^T \boldsymbol{\sigma}\, \mathrm{d}V + \int_V \delta\varepsilon^T \boldsymbol{\sigma}_\vartheta\, \mathrm{d}V + \\ + \int_V \delta\boldsymbol{u}^T \ddot{\boldsymbol{u}}\, \rho \mathrm{d}V = \sum_i \delta\boldsymbol{u}^T \boldsymbol{f}_i\,, \tag{16}$$

where ε denotes the strain and $\boldsymbol{\sigma}$ the stress field. $\boldsymbol{f}_i$ represent the applied external forces.

3.3 Modal Approach

Again a Ritz approximation is used to discretize the deformation field $\boldsymbol{u}$:

$$\boldsymbol{u}(\boldsymbol{c},t) = \boldsymbol{\Phi}_u(\boldsymbol{c})\boldsymbol{z}_u(t) \tag{17}$$

The spatial shape functions in (17) are formulated as function of cylindrical coordinates, i.e. $\boldsymbol{\Phi}_u = \boldsymbol{\Phi}_u(r,\phi,z)$, $w_{,r}$ and $w_{,\phi}$ are partial derivatives with respect to r or ϕ:

$$\sum_{i=1}^{n} \boldsymbol{\Phi}_{ui} z_{ui} = \begin{bmatrix} -z(\cos(\phi) w_{,r} - \frac{\sin(\phi)}{r} w_{,\phi}) \\ -z(\sin(\phi) w_{,r} + \frac{\cos(\phi)}{r} w_{,\phi}) \\ w \end{bmatrix},$$

$$w = \sum_{l=0}^{l_m} \sum_{k=0}^{k_m} R_l(r) \cdot \cos(k\phi) \cdot z_{ui}(t) + \ldots \\ \ldots + \sum_{l=0}^{l_m} \sum_{k=1}^{k_m} R_l(r) \cdot \sin(k\phi) \cdot z_{ui}(t)\,, \tag{18}$$

$$\text{with } i = 1,2,\ldots,n\,,\ n = (l_m+1)(2k_m+1)\,.$$

The trial functions in (18) correspond to the trial functions in (5) except of the fact, that a 2-dimensional field is discretized here, while the temperatures depend on all three coordinates.

3.4 Discretized Field Equations

If (18) is inserted into (16) the linear field equation for the displacements is yielded:

$$\boldsymbol{M}_{uu}\ddot{\boldsymbol{z}}_u + \boldsymbol{C}_{uu}\dot{\boldsymbol{z}}_u + \boldsymbol{K}_{uu}\boldsymbol{z}_u + \boldsymbol{K}_{u\vartheta}\bar{\boldsymbol{z}}_\vartheta = \sum_i \boldsymbol{\Phi}_{ui}^T \boldsymbol{f}_i\,. \tag{19}$$

The mass matrix $\boldsymbol{M}_{uu}$ in (19) denotes the volume integral

$$\boldsymbol{M}_{uu} := \int_V \boldsymbol{\Phi}_u^T \boldsymbol{\Phi}_u\, \rho \mathrm{d}V\,, \tag{20}$$

the stiffness matrix $\boldsymbol{K}_{uu}$ is defined using the linear displacement-strain operator ∇_u, the abbreviation $\boldsymbol{B}_u := \nabla_u \boldsymbol{\Phi}_u$ and the elasticity tensor $\boldsymbol{H}$:

$$\boldsymbol{K}_{uu} := \int_V \boldsymbol{B}_u^T \boldsymbol{H} \boldsymbol{B}_u\, \mathrm{d}V\,. \tag{21}$$

As usual, the introduction of the damping matrix $\boldsymbol{C}_{uu}$ as an assembly of mass and stiffness terms is justified by empirical considerations [12, Sec. 4.2]. The thermo-elastic coupling matrix follows from (15):

$$\boldsymbol{K}_{u\vartheta} := \int_V E\alpha \frac{1+\nu}{1-\nu^2} \cdot \\ \cdot \left(\boldsymbol{\Phi}_{u,rr} + \frac{\boldsymbol{\Phi}_{u,r}}{r} + \frac{\boldsymbol{\Phi}_{u,\phi\phi}}{r^2} \right)^T z\, \boldsymbol{\Phi}_\vartheta\, \mathrm{d}V \tag{22}$$

In addition to the deformations, the motion of the disc's reference frame located at the center of gravity is considered by the Newton-Euler equations [21, (8.6),(8.21)]:

$$m \cdot \boldsymbol{a} = \sum \boldsymbol{f}_i\,, \\ \boldsymbol{I}\dot{\boldsymbol{\omega}} + \boldsymbol{\omega} \times \boldsymbol{I}\boldsymbol{\omega} = \sum \boldsymbol{c}_i \times \boldsymbol{f}_i + \sum \boldsymbol{p}_i\,. \tag{23}$$

$\boldsymbol{a}$ denotes the translational acceleration of the reference frame, $\boldsymbol{\omega}$ its rotational velocity. $\boldsymbol{I}$ symbolizes the interia tensor, m its mass. $\boldsymbol{f}_i$ presents the discrete external forces, $\boldsymbol{p}_i$ discrete external torques.

4 User Interface

4.1 The Icon Layer

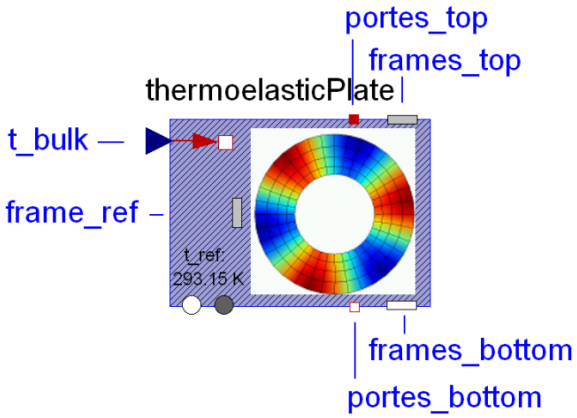

Figure 3: Icon layer of the ThermoelasticPlate class.

The icon layer of ThermoelasticPlate class is shown in Fig. 3. The connector arrays *frames_top* and *frames_bottom* both represent points that slide on the

upper or the lower surface of the plate, respectively and therefore are potential connectors to apply brake forces. The associated heat fluxes generated by friction may be applied to the companion heat port arrays *portes_top* and *portes_bottom*. Each of these arrays contains as much connectors as are specified by the first dimension of the input parameter *xsi* in the following table:

geometrical parameters		
r_i	$[m]$	inner radius of the plate
r_a	$[m]$	outer radius of the plate
$th[:]$	$[m]$	thickness of the plate
$xsi[:,2]$	$[-]$	points on the disc

Each row of *xsi* specifies the radial and the angular position of two surface points with respect to the frame $\mathcal{A}$ in Fig. 2 parametrized in the interval $[0,1]$. E.g. $xsi[1,:] = \{0.5, 0.125\}$ defines two surface points in the middle between the inner and outer radius at 45° angular position.

In addition to the 3-dimensional multibody frame connectors, two 1-dimensional rotational flanges are shown in Fig. 3. These two flanges are connected to both sides of the 3-dimensional rotational joint which is introduced into the ThermoelasticPlate class at the plate axis by default. The two flanges are conditionally instantiated controlled via user parameter and can be utilized to e.g. define constant rotation velocity.

4.2 The Physical Parameters

The thermal field equations (6) are formulated with respect to a reference temperature *t_ref*, which may be interpreted as linearisation point at which all physical material parameters are specified. *t_ref* is as well defined by user input and displayed in the icon layer as shown in Fig. 3. Since the model also considers cooling by air convection, another input is necessary to provide information on the bulk temperature *t_bulk*, which is interpreted relative to the reference temperature *t_ref*.

The table below shows the thermal parameters the user has to provide in order to employ a ThermoelasticPlate instance:

thermal parameters		
$rho[:]$	$[kg/m^3]$	mass density
$lamdba[:,3]$	$[W/mK]$	thermal conductivity
c	$[K/kgK]$	specific heat capacity
hf_{outer}	$[W/m^2K]$	convective heat coeff.
hf_{inner}	$[W/m^2K]$	convective heat coeff.
$alpha$	$[1/K]$	thermal expansion coeff.

The physical properties are assumed to be homogeneous in radial and tangential direction, while different sections may be defined in axial direction. This is why the geometrical input parameter *th* is defined as a vector. E.g. the values $th = \{0.003, 0.007, 0.01\}$ specify three thickness sections from 0 to 3 mm, from 3mm to 7 mm and from 7 to 10mm.

As a consequence, the input dimensions of *th*, *rho*, *lambda* and the Young's modulus E to be introduced below are related, since e.g. the density *rho[1]* is supposed to specify the mass density in the first section, i.e. is assigned to the thickness region from 0 to 3 mm for the given example of *th*. Each column of the parameter *lambda*, i.e. *lambda[:,i]* is also related to the section from *th[i-1]* to *th[i]*, while the first element *lambda[1,i]* specifies the thermal conductivity in radial, the second element *lambda[2,i]* in axial and the third element *lambda[3,i]* in tangential direction.

By this set-up it is intended to approximately account for a brake disc design as it is shown in Fig. 4. The reduced heat capacity of the center region with the cooling channels may be considered by a reduced mass density. An appropriate definition of lambda specifies heat conduction in the center region only to occur in axial but not in radial or tangential direction. The coefficient hf_{inner} quantifies the heat transfer from the brake disc to the circulating air at the areas with *th[i]=0.003* and *th[i]=0.007* in the given example of *th*. The input parameter hf_{outer} refers to the convective heat transfer at both outer surfaces of the brake disc.

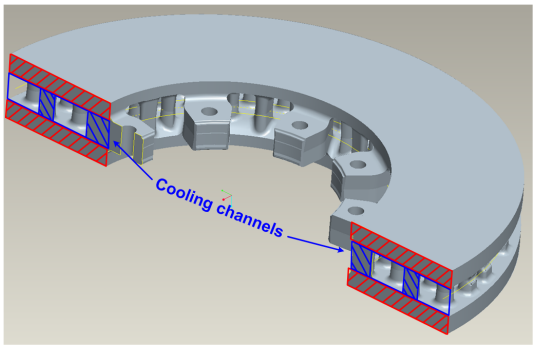

Figure 4: Cooling channels in a brake disc.

The mechanical parameters have to be given as follows:

mechanical parameters		
$E[:]$	$[N/m^2]$	Youngs's modulus
ny	$[-]$	Poisson number
$damping$	$[-]$	natural damping coefficient

The Young's modulus E as a function of the thickness coordinate *th* is used to evaluate the flexural rigid-

ity of the Kirchhoff plate according to the theory of multi-layered plates [22, 3.7] in order to reflect the influence of the cooling channels on the bending behavior.

If (19) is given in normal or principal coordinates, see e.g. [23, 6.5], the homogeneous equations of motion will be separated in independent equations of the following typ:

$$\ddot{z}_{u,i} + 2\delta_i \omega_i \dot{z}_{u,i} + \omega_i^2 z_{u,i} = 0 \qquad (24)$$

with the eigenvalue ω_i and the natural damping coefficient δ_i. The input parameter *damping* controls the assembly of the damping matrix $\boldsymbol{C}_{uu}$ in such a way that δ_i equals *damping* for all normal coordinates. As a default value *damping=1* is specified which corresponds to critical damping. This set-up follows the assumption that thermoelastic deformations and external excitations act in a frequency range much lower than the first natural frequency of the plate and inertia effects may be neglected. However, it is up to the user to define alternative damping regimes by giving other values for *damping*.

4.3 The Discretization Set-up

The input parameter vector *th* implicitly also rules the discretization of the thermal field in axial direction, which is done by B-spline functions, see Fig. 1. In this context, the parameter values of *th* are interpreted as elements of the so-called knot vector [15]. Depending on the dimension of *th*, constant, linear, quadratic or cubic B-splines are applied.

The discretization of the thermal field in radial direction is specified by the input parameter *radialDiscretization*, which directly defines the number of degrees of freedom in radial direction. Due to the B-spline concept the order of the trial-functions is associated to the number of degress of freedom, so that the following relations hold:

radialDiscretization	B-spline type
1	constant
2	linear
3	linear
4	linear
5	quadratic
6	quadratic
≥ 7	cubic

In principle the parameter *radialDiscretization* also counts for the mechanical field with one exception: exclusively cubic B-spline functions are used to describe the bending deformations with respect to the radius. If necessary to satisfy this basic demand additional number of degrees of freedom are introduced for the mechanical field in addition to the input specification of *radialDiscretization*.

The integer parameter vector *angularDiscretization* contains the ordinal numbers of the Fourier terms k from (5) which are to be considered in order to describe the thermal and the mechanical field in circumferential direction.

Finally, the user has to choose the boundary condition for the displacement field at the inner radius out of two options, namely *supported* or *clamped*.

5 Simulation Example

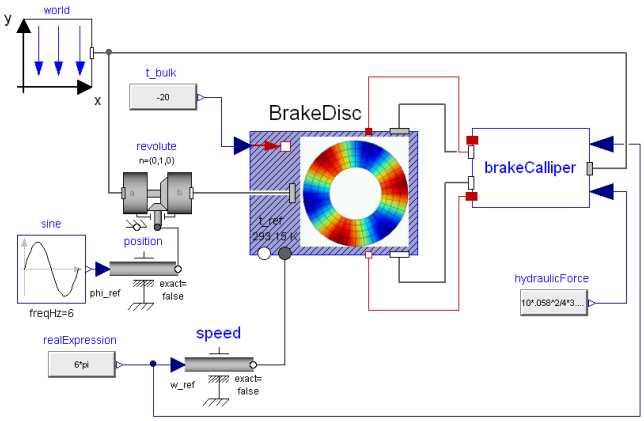

Figure 5: Diagram layer of the brake model.

The example shown in Fig. 5 is a representation of a braking system which illustrates an application of the thermo-elastic plate model. The model contains a floating caliper with brake pads sliding along both sides of the brake disc. A constant rotation velocity of 6π rad/s and a constant hydraulic force are specified. An axial run-out of the brake disc is simulated since the disc is tilted around its y-axis with 0.005 rad amplitude and 6 Hz, see the revolute joint in Fig. 5. A constant friction coefficient of $\nu = 0.9$ assumed. The brake disc is 10 mm thick, 70 mm and 120 mm are specified as inner radius and outer radius, and its physical parameters correspond to cast iron material.

A second order Fourier expansion is applied to discretize both fields in circumferential direction, four linear B-splines are used for the axial discretization, three linear B-splines for the radial discretization of the thermal field.

The disc-pad contact is defined at 9 points at each side of disc, which are located at $-28.8° \leq \theta \leq 28.8°$

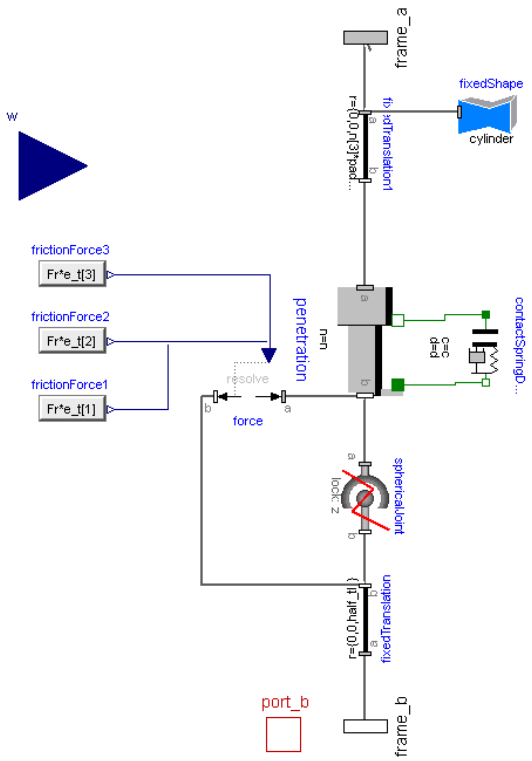

Figure 6: Diagram layer of the contact submodel.

angular position. The contact is formulated with one prismatic joint in axial direction for each contact point. *frame_a* in Fig. 6 is supposed to provide the connection to the brake caliper, *frame_b* is to be connected to one frame at the surface of the thermoelasticPlate, *port_b* is the associated heat port to define the heat flow into the brake disc.

In addition the variable *port_b.T* represents the temperature at the contact point and might be used to formulate e.g. temperature-dependent friction behavior in future scenarios. Secondary heat flows e.g. to the caliper body or thermal contact resistances may be included into this configuration as well. Even phenomena such as brake fluid boiling [4] may be investigated by appropriate straight-forward model extensions.

The non-linear spring-damper element attached to the prismatic joint represents the contact stiffness and is capable to consider the loss of contact or the lift-off of the brake pads, respectively. However this effect is not part of the presented simulation scenario. The simplicity of the contact modeling here again demonstrates the advantages of the Eulerian description.

Fig. 7 presents an animation of the simulation scenario. The green arrows visualize the friction forces, the color of the plate surface indicates the temperature distribution, which in general exposes a maximum at the trailing edge of the brake pads.

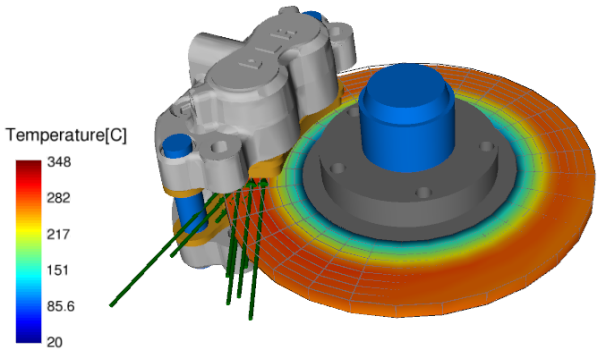

Figure 7: Animation of the brake model.

The exciation by the axial run-out leads to oscillations of the normal and tangential forces inversely phased on the top and the bottom surface of the brake disc. The influence of this excitation on the thermal field is presented by the curves in Fig. 8. The detailed plot below reveals a antisymmetric pattern of the temperature distribution at both surfaces of the brake disc, although the actual temperature differences are indeed small. In addition the general temperature rise is stepped by the rotation frequency of the brake disc.

Another result of the axial run-out is shown in Fig. 9, where the bending deformations at the outer radius at $\theta = 0°$ angular position are plotted as a function of time.

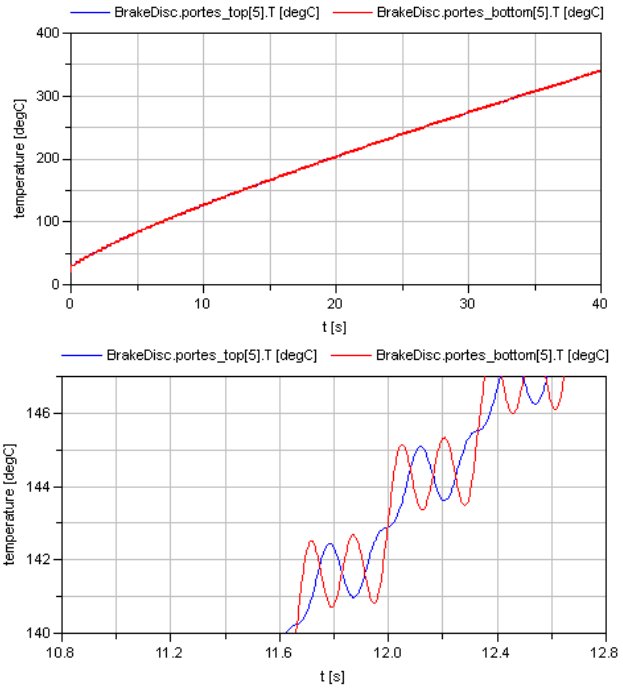

Figure 8: Exemplary temperature results at the top and the bottom surface, $r = 0.102$ m, $\theta = 0°$.

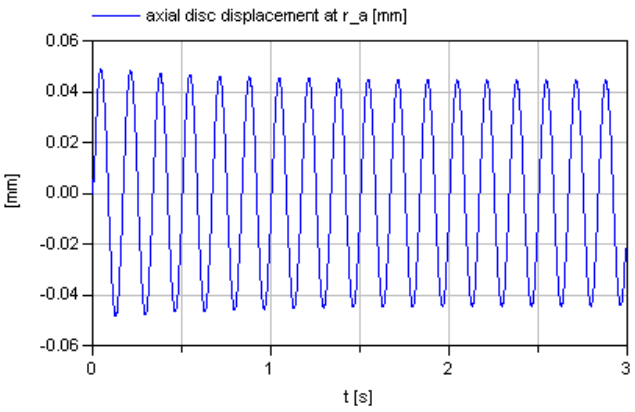

Figure 9: Plot of the plate deformation at the outer radius at $\theta = 0°$ angular position.

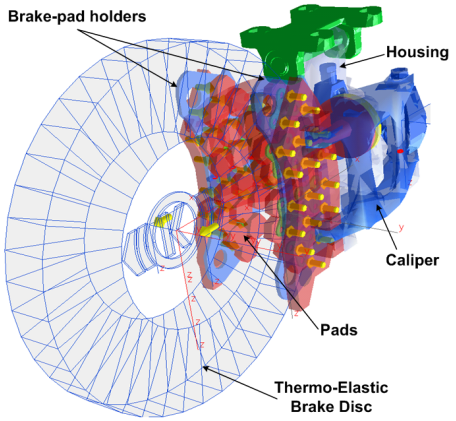

Figure 10: Braking mechanism of a train.

It should be mentioned that these preliminary results still must be validated. Nevertheless the results can be interpreted in a physical way and are plausible.

The brake disc model considers 60 thermal and 30 mechanical degrees of freedom and 106 cpu-s on a common laptop are spent to simulate the scenario with 40 s simulation time.

6 Conclusions and Outlook

The present paper introduces a new Modelica class called ThermoelasticPlate. This model is tailored to represent the thermal and thermo-elastic behavior of brake discs in the lower frequency range. The advantages of the Eulerian approach are exploited, so that the non-rotating normal and friction forces and the associated heat fluxes may easily be applied.

An example study demonstrates the application of the new Modelica class. Although validation of the presented analysis is still a pendent task, the results however have shown a good agreement with the physical description of this phenomenon giving a solid basis to cope with some of the most common braking problems such as hot spotting. It has been demonstrated that the approach is open for a wide range of application scenarios such as temperature-dependent friction and brake-fluid boiling.

Moreover, the purpose of this project is to integrate the thermo-elastic model into more complex scenarios, such as a complete braking system of a train (Figure 10) which includes brake disc (thermo-elastic model), brake pads, rockers, brake pad holders, calipers, housing, brake piston, etc., in order to analyze the induced vibrations, due to the thermo-mechanical deformations, into the complete dynamics of the entire system.

7 Acknowledgements

The authors highly appreciate the partial financial support of Knorr-Bremse Systems for Railway Vehicles in Munich.

References

[1] S.K. Rhee. Friction coefficient of automotive friction materials – its sensitivity to load, speed, and temperature. *SAE Technical paper 740415*, 1974.

[2] S. Panier, P. Dufrénoy, and D. Weichert. An experimental investigation of hot spots in railway disc brakes. *Wear*, 256:764 – 773, 2004.

[3] T.K. Kao, J.W. Richmond, and A. Douarre. Thermo-mechanical instability in braking and brake disc thermal judder: an experimental and finite element study. In *Proc. of 2nd International Seminar on Automotive Braking, Recent Developments and Future Trends, IMechE*, pages 231–263, Leeds, UK, 1998.

[4] K. Lee. Numerical prediction of brake fluid temperature rise during braking and heat soaking. *SAE Technical Paper 1999-01-0483*, 1999.

[5] A. Rinsdorf. *Theoretische und experimentelle Untersuchungen zur Komfortoptimierung von Scheibenbremsen*. Höppner und Göttert, Siegen, 1996.

[6] T. Steffen. *Untersuchung der Hotspotbildung bei Pkw-Bremsscheiben*. Number 345 in VDI–Fortschrittsberichte Reihe 12. VDI-Verlag, Düsseldorf, 1998.

[7] T. Tirovic and G.A. Sarwar. Design synthesis of non-symmetrically loaded high-performance disc brakes, Part 2: finite element modelling. *Proc. of the I Mech E Part F: Journal of Rail and Rapid Transit*, 218:89 – 104, 2004.

[8] P. Dufrénoy. Two-/three-dimensional hybrid model of the thermomechanical behaviour of disc brakes. *Proc. of the I Mech E Part F: Journal of Rail and Rapid Transit*, 218:17 – 30, 2004.

[9] K. Lee and J.R. Barber. Frictionally excited thermoelastic instability in automotive disk brakes. *Journal of Tribology*, 115:607 – 614, 1993.

[10] C. Krempaszky and H. Lippmann. Frictionally excited thermoelastic instabilities of annular plates under thermal pre-stress. *Journal of Tribilogy*, 127:756–765, 2005.

[11] B.A. Boley and J.H. Weiner. *Theory of Thermal Stresses*. Dover Publications, Mineola, New York, 1997.

[12] H.J. Bathe. *Finite Element Procedures*. Prentice Hall, New Jersey, 1996.

[13] R.W. Lewis, K. Morgan, H.R. Thomas, and K.N. Seetharamua. *The Finite Element Method in Heat Transfer Analysis*. John Wiley and Sons, Chichester, UK, 1996.

[14] W. Ritz. Über eine neue Methode zur Lösung gewisser Variationsprobleme der mathematischen Physik. *Journal für Reine und Angewandte Mathematik*, 135:1–65, 1908.

[15] Carl de Boor. *A practical Guide to Splines*. Springer–Verlag, Berlin, 1978.

[16] A. Heckmann. *The Modal Multifield Approach in Multibody Dynamics*. Number 398 in Fortschritt-Berichte VDI Reihe 20. VDI-Verlag, Düsseldorf, 2005. PhD thesis.

[17] J. Salençon. *Handbook of Continuum Mechanics*. Springer-Verlag, Berlin, 2001.

[18] A. Heckmann, S. Hartweg, and I. Kaiser. An Annular Plate Model in Arbitrary Lagrangian-Eulerian-Description for the DLR FlexibleBodies Library. In *8th International Modelica Conference*, 2010. submitted for publication.

[19] O. Wallrapp and R. Schwertassek. Representation of geometric stiffening in multibody system simulation. *International Journal for Numerical Methods in Engineering*, 32:1833–1850, 1991.

[20] F. Bloom and D. Coffin. *Handbook of Thin Plate Buckling and Postbuckling*. Chapman & Hall/CRC, Washington, D.C., 2001.

[21] P.E. Nikravesh. *Computer-aided Analysis of Mechanical Systems*. Prentice Hall, Engelwood Cliffs, New Jersey, 1988.

[22] R. Szilard. *Theory and Analysis of Plates*. Prentice-Hall, Inc., Englewood Cliffs, New Jersey, 1974.

[23] L. Meirovitch. *Computational methods in structural dynamics*. Sijthoff & Noordhoff, Alphen aan den Rijn, Netherlands, 1980.